

Dynamics of vitrimers: defects as a highway to stress relaxation

Simone Ciarella,¹ Francesco Sciortino,² and Wouter G. Ellenbroek^{1,3}

¹*Department of Applied Physics, Eindhoven University of Technology,
Postbus 513, NL-5600 MB Eindhoven, Netherlands*

²*Department of Physics and CNR-ISC, Sapienza Università di Roma, Piazzale Aldo Moro 2, I-00185 Roma, Italy*

³*Institute for Complex Molecular Systems, Eindhoven University of Technology,
Postbus 513, NL-5600MB Eindhoven, The Netherlands*

(Dated: March 15, 2022)

We propose a coarse-grained model to investigate stress relaxation in star-polymer networks induced by dynamic bond exchange processes. We show how the swapping mechanism, once activated, allows the network to reconfigure, exploring distinct topological configurations, all of them characterised by complete extent of reaction. Our results reveal the important role played by topological defects in mediating the exchange reaction and speeding up stress relaxation. The model provides a representation of the dynamics in vitrimers, a new class of polymers characterized by bond swap mechanisms which preserve the total number of bonds, as well as in other bond-exchange materials.

PACS numbers: 82.35.Lr, 05.10.-a, 83.10.Rs

Vitrimers, an exciting new class of polymer networks, are unique in their ability to interpolate between the two conventional classes of polymer, thermoplastics and thermosets [1]. The first can be reshaped at will, but are sensitive to being weakened by contact with solvents, while the latter are insoluble but cannot be reshaped after the cross-linking process. In vitrimers, a connectivity-preserving bond exchange mechanism [2–5] with well-controlled exchange rate makes the cross-links dynamic. At low rates, they perform like thermosets, while at high rates, they are malleable like thermoplastics. Unlike permanently cross-linked elastomers or gels, these bond swaps allow vitrimers to release internal stresses without losing shape. Their versatility shines particularly in smartly designed materials, where bond swapping provides a welding strategy [6], or responsiveness to light, pH, voltage, metal ions, redox chemicals and mechanical stimuli [7–9].

The unusual molecular interaction in vitrimers renders current theories of polymer performance of limited use. Neither a conventional static model nor a fully dynamic one can coherently address the exchange dynamics. At the atomistic level, exchange reactions can be effectively modeled using reactive force fields [10]. This gives a detailed picture of a single exchange event, but does not provide large enough time and length scales to assess macroscopic properties. To get to macroscopic scales, a coarse-grained model that captures the network-topology aspects of the exchange reactions is needed.

In recent years, scientists have developed different numerical models to study exchange materials [11–13], embedding Monte Carlo hopping moves into hybrid molecular dynamics or Monte Carlo (MD,MC) simulations to reproduce bond swaps. In this letter, we study a vitrimer model consisting of associative star-polymers using a three-body potential to reproduce bond exchange dynamics with a controllable rate [14], avoiding the need for

hybrid features. Using molecular dynamics simulations to obtain the stress relaxation modulus, we verify the expected transition from solid-like to liquid-like long-time behavior upon increasing the bond exchange rate [15]. More importantly, we uncover a dramatic difference in stress relaxation that arises from the molecular topology. In close connection to recent work that demonstrated how loops affect equilibrium elastic properties [16], we show that networks made from building blocks that allow loop formation via bond exchange relax stresses much faster than systems made from loop-preventing building blocks, even when the bond exchange rates are the same. Thus, the slow relaxations that characterize swapping vitrimers [17] can be controlled not only through the swap rate, but also through defect formation. In this sense, loop defects serve as highways to stress relaxation, giving faster self-healing and better malleability and recyclability [4, 12]. Combining this effect with an accurate choice of the network topology we can imagine to synthesize a material which is not only stable as thermosets and malleable as thermoplastics, but also tougher than either, because it can relax stresses in a controllable way, while having improved structural integrity compared to materials toughened via other mechanisms such as fully reversible crosslinking [18] or sacrificial bonds [19].

Modeling Vitrimers—We focus our simulations on networks built from binary mixtures of eight-arm star polymers. Each arm terminates with a reactive site which can be of two different types, labeled red and blue (see Fig. 1(a)). This effectively captures what happens in vitrimers that rely on covalent association of two different moieties, via e.g. ester bonds [4, 5], in which case the end types represents carboxyl and hydroxyl groups, respectively. Star-shaped monomers are widely used polymeric building blocks, for e.g. dendrimers and tetra-PEG hydrogels [20, 21]. They are a versatile basis for covalent adaptive networks, with controlled connectivity and ar-

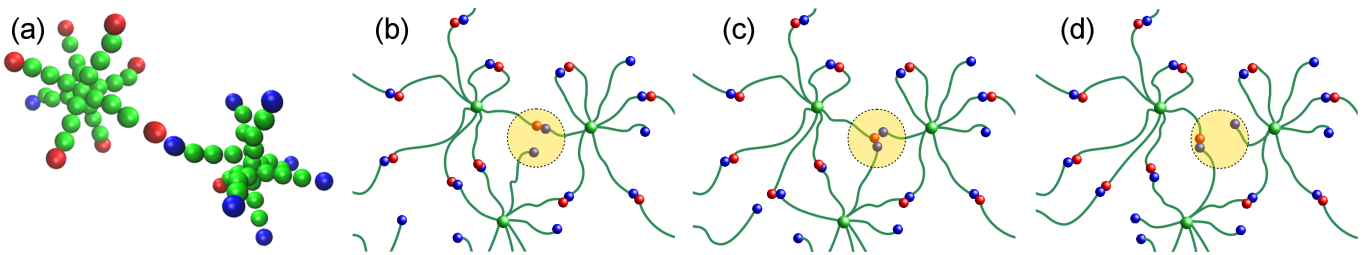


FIG. 1. (a) Our star-shaped monomers forming a swappable covalent bond (red-blue). (b)-(d) Sketch of a swap event: red-blue bonds can swap, while green beads are permanent links (the centers of the stars). The swap reaction modifies the topology of the network. Its rate is catalytically controlled in real systems, modeled here by tuning the energy barrier. In states (b) and (d) there is only a two-body energy term ($\approx -\epsilon$) due to the highlighted bond. In state (c) there are two two-body energy terms ($\approx -2\epsilon$) and one three-body contribution ($\approx +\lambda\epsilon$). If $\lambda = 1$, the three-body term compensates exactly the formation energy of the second bond effectively flattening out the energy barrier.

chitecture [2].

We coarse grain the star-polymer as a sequence of beads and harmonic springs [22] with a rest length of 1 nm which is our unit of length. The beads, shown in green in Fig. 1(a), thus represent Kuhn segments consisting of roughly 8 carbon atoms. Masses, energies and times are expressed in units $[m] = 100 \text{ u}$, $[E] = k_B \cdot 300 \text{ K}$, and $[\tau] = 6.33 \text{ ps}$, respectively. All pairs of beads interact via a purely repulsive WCA potential ($\sigma = 1 \text{ nm}$) [23].

Modelling swappable covalent bonds using potentials requires care. They must enforce single red-blue bonds without clustering, contain a parameter to tune the swap rate, and the bonds they provide must be thermally stable. To this end, we use a combination of two-body and three-body interactions as proposed in Ref. [14]. The two-body term is a generalized Lennard-Jones potential acting only between red-blue pairs,

$$v_{ij}(\vec{r}_{ij}) = 4\epsilon \left[\left(\frac{\sigma}{r_{ij}} \right)^{20} - \left(\frac{\sigma}{r_{ij}} \right)^{10} \right] \quad r < r_{\text{cut}} . \quad (1)$$

With $\sigma = 0.5 \text{ nm}$ and $\epsilon = 100 k_B T$, the $v_{ij}^{(2b)}$ provide a covalent-like bond that is stable against thermal fluctuations. We fix $r_{\text{cut}} = 2.5\sigma$. The 3-body term is rewritten in terms of how the interaction between particles i and j is affected by the presence of other particles k that are within range of particle i ,

$$v_{ijk}^{(3b)} = \lambda\epsilon \hat{v}_{ij}^{(2b)}(\vec{r}_{ij}) \cdot \hat{v}_{ik}^{(2b)}(\vec{r}_{ik}) , \quad (2)$$

where $\lambda \geq 1$ is the three-body scaling parameter and $\hat{v}_{ij}^{(2b)}$ is defined as

$$\hat{v}_{ij}^{(2b)}(\vec{r}_{ij}) = \begin{cases} 1 & r \leq r_{\text{min}} \\ -\frac{v_{ij}(\vec{r}_{ij})}{\epsilon} & r > r_{\text{min}} . \end{cases} \quad (3)$$

Because it is formulated in terms of the attractive part of the two-body term, this three-body potential compensates the pair energy that would be gained by two simultaneous red-blue bonds so that all intermediate states

encountered during a swap event are similar in potential energy. This flat energy landscape is the defining feature of the method, as illustrated in Fig. 1(b-d). The three-body term automatically enforces the single-bond per reactive site since it gives a strong repulsion when more than 3 reactive sites are close. The parameter λ sets the energy barrier for a swap rearrangement ΔE_{sw} . To a first approximation $\beta\Delta E_{\text{sw}} \equiv \beta\epsilon(\lambda-1) = 100(\lambda-1)$.

While three-body interactions are generally expensive in simulations, Eq. (2) requires only small additional numerical effort compared to a standard two body potential, because it is a combination of the existing two-body terms.

Numerical approach—We use the Hoomd-blue package [24, 25] to do molecular dynamics simulations on GPUs. For the three-body potential, we developed a Hoomd-blue module named “RevCross”. This implementation allows us to gather sufficient statistics for evaluating the stress relaxation in systems of $N \approx 50000$ beads (≈ 1500 star polymers). To provide a reservoir of open endings that can initiate a swap event we use a non-stoichiometric mixture of different star endings, following the chemistry behind vitrimers. We exploit two different mixtures to assess the role of defects (loops) in the stress relaxation.

We focus on the type of defects known as primary loops, in which two endings of the same star are bonded together. These are the most important for the static elastic properties [16]. First, we employ a defect-free mixture (DFM) composed of $N_A = 900$ 8-arm star polymers whose endings are only type A and $N_B = 600$ stars with only B-type ends. Since A–B bonds are allowed, primary loops are prevented. Later, we present results on a defect-allowing mixture (DAM) which contains $N_A = 950$ stars with seven A-type endings and a single B-type ending, and $N_B = 550$ stars with the numbers reversed. These values of N_A and N_B make the total number of red and blue beads identical in both mixtures. Since the red-blue bonds are much stronger than $k_B T$, all 4800 B-type ends will form a bond, leaving 2400 free A-type ends available

to initiate swap events. The large number of arms is used in order to have a network that behaves like a solid without applying any (osmotic) stretching. Both networks are equilibrated in periodic cubic boxes of size $L = 40$ nm, corresponding to a packing fraction $\phi \approx 0.3$. This corresponds to 2.2 times the overlap concentration, so the stars can easily form a network, but it is low enough to avoid any glassy dynamics. In the supplementary information, we demonstrate that indeed there is no caging or segmental slowing down at this density, so that the polymer arms are mobile enough to initiate bond swaps [26]. For both DFM and DAM mixtures, we generate $m = 100$ independent network topologies.

Stress relaxation—We perform stress relaxation calculations. Rather than doing out of equilibrium MD calculating the stress $\sigma(t)$ after a step strain, we exploit the widely used autocorrelation method

$$G(t) \approx C(t) \equiv \frac{V}{k_B T} \left\langle \overline{\sigma_{yz}(t)\sigma_{yz}(0)} \right\rangle \quad (4)$$

in the nVT ensemble where we imposed the number of stars n , the volume V , and the temperature T . The bar and brackets denote averaging over time and ensemble, respectively. To calculate the instantaneous stress $\sigma(t)$ we have to add terms that arise from the three-body potential to the standard (pair-based) virial expression. In the SI [26], we derive these terms from the thermodynamic definition of stress.

The stress autocorrelation function is often assumed to be equal to the stress relaxation $G(t)$, but it was recently pointed out that the equality holds only in liquids [27, 28]. Still, for self-assembled networks, $C(t)$ on average converges to $G(t)$ [11]. The correct way to define the stress relaxation would be

$$G(t) = \begin{cases} C(t), & \text{liquids} \\ C(t) + G_{\text{eq}} - C_{\infty}, & \text{solids} \end{cases} \quad (5)$$

where G_{eq} is the shear modulus and C_{∞} is the long-time asymptote of $C(t)$ (so $C_{\infty} \propto \langle \bar{\sigma} \rangle^2$). Thus, the stress autocorrelation function $C(t)$ and the stress relaxation modulus $G(t)$ always coincide in the liquid phase, but when the system rigidifies, $C(t)$ shifts from $G(t)$ by a constant [27]. While they become identical only in thermodynamic limit [11], we can distinguish a solid from a liquid using the limiting behavior of $C(t)$, even in a finite ensemble. The reason this works is that the only way to have $C_{\infty} = 0$ is when $\bar{\sigma} = 0$ for every configuration, which happens only for liquids. In the following we will simply use $C(t)$.

Swap-driven transition without loops—The stress relaxation for the DFM system is reported in Fig. 2a. We define τ_{net} as roughly the time that it takes for a solid network to reach its elastic plateau, $\tau_{\text{net}} \approx 5$ ns. At short times ($t < \tau_{\text{net}}$), the stress relaxation is dominated by the Rouse modes of the chains [29]. We refrain from

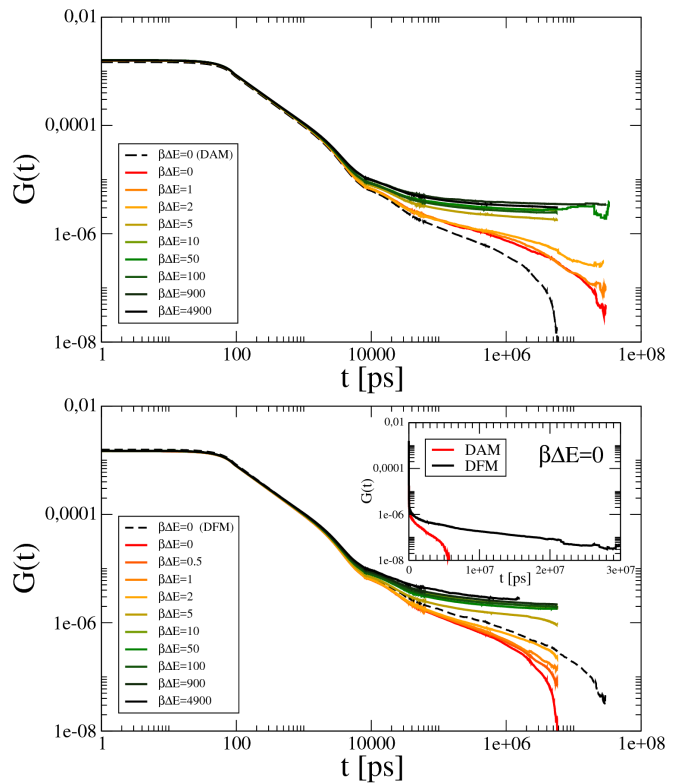


FIG. 2. (a) Stress relaxation for the Defect Free Mixture (DFM), for a range of swap barrier values (DAM data shown as dashed line for comparison). (b) Stress relaxation for the Defect-Allowed Mixture (DAM), with DFM data shown as dashed line for comparison. After the first regime of relaxation due to chain rearrangement, a solid plateau is approached. For low enough energy barriers, swap rearrangements trigger a second relaxation. This network relaxation is an order of magnitude faster with defects than without. Inset: DAM-DFM comparison on a linear time axis.

fitting a power law to this regime because the arms of the star polymers are too short to make this feasible. All curves coincide until this timescale because swapping is slow and the network topology is essentially fixed. Then the gel starts sustaining the stress and a plateau in $G(t)$ appears. If the swap move has a large energy barrier ($\beta\Delta E_{\text{sw}} > 50$), the topology remains fixed and the plateau extends beyond times reachable by simulation. If instead the gel rearranges through bond swap moves, we observe a second relaxation, the hallmark of transient networks [11–13, 30]. We conclude that when there is no activation barrier, swaps make DFM liquid at $\tau_{\text{liq}}^{\text{DFM}} \approx 20 \mu\text{s}$, where we picked $G(\tau_{\text{liq}})/G(0) \equiv 10^{-4}$.

Swap-driven transition with loops—The stress relaxation for the DAM system is reported in Fig. 2b. After chain relaxation, the solid plateau is approached only by the fixed networks, while the swapping ones keep relaxing all of their stress. In this mixture, bond swapping contributes to stress relaxation on shorter time scales. In marked contrast with the system without loop de-

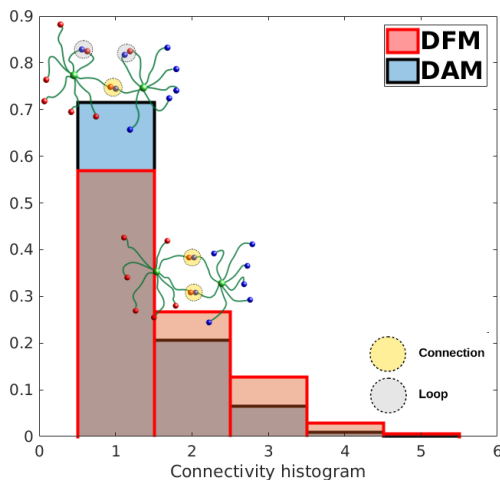


FIG. 3. Histogram of the number of connections between connected stars, for both mixtures. In the DAM (blue), the presence of loops causes the average number of connections between stars to be lower. This reduces redundancy and thereby increases the chance that a single swap even will disconnect two stars, which speeds up stress relaxation.

fects, the final stress relaxation is now ten times faster, $\tau_{\text{liq}}^{\text{DAM}} \approx 0.1 \cdot \tau_{\text{liq}}^{\text{DFM}} \approx 2 \mu\text{s}$. The swapping gel with defects behaves essentially like a viscous liquid.

To rule out that the faster stress relaxation is caused by structural quantities unrelated to loop defects, we verified that all 2400 possible bonds formed in both mixtures, and that the number of swap events is similar in both. Finally, we checked that the DAM mixture indeed formed loop defects, and found that typically between 1/5 and 1/3 of all bonds in this mixture are primary loops, connecting two arms of the same star.

The conclusion is that the fast stress relaxation of the defect-allowing mixture is caused by “defected” configurations. Whenever an intra-star bond that was carrying stress is swapped with an arm on the same star to form a defect, it ceases to support stress, giving rise to dissipation. This consistently leads to fewer redundant connections between stars, as we show in Fig. 3, which in turn makes the fraction of swap events that actually detach two stars even larger, leading to more relaxation per event. Given that the swap rate is similar for the two mixtures, this means the defects act as a highway to stress relaxation.

Discussion—We have shown the effectiveness of MD simulations in the study of bond swapping systems. The employed three-body potential turns bond-swap events into a continuous process: Free binding sites approach an existing bond via a tunable barrier, and after the exchange the unbound partner leaves via the same pathway. The computational effort of evaluating a three-body interaction is partly mitigated by defining it in terms of pair forces which had to be computed anyway. Compared to Monte Carlo moves for bond exchanges, our approach

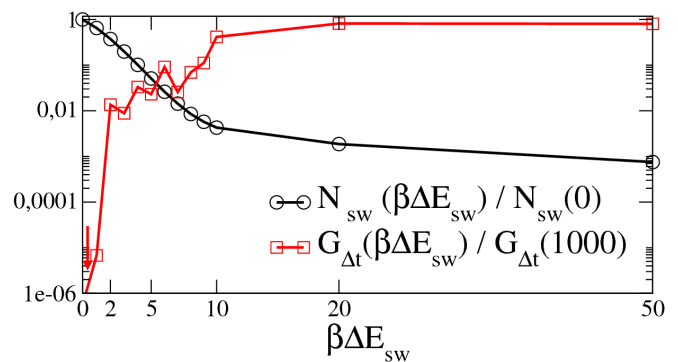


FIG. 4. Normalized number of swaps (black) and stress relaxation (red) as a function of the swap energy barrier $\beta\Delta E_{\text{sw}}$, for the DAM system. The fluid-solid transition happens when the barrier is $10k_B T$.

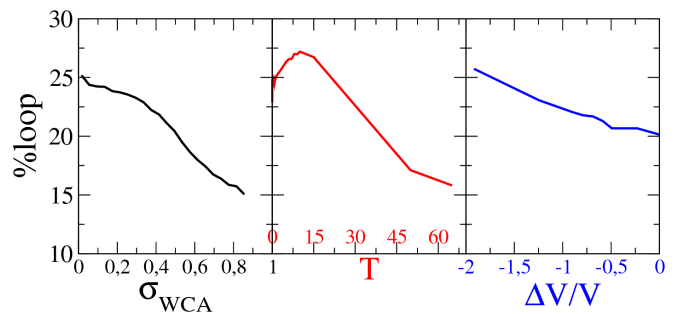


FIG. 5. We can control the number of loop defects by inflating the monomers (black), increasing temperature (red), or volumetric compression (blue).

has the advantage that dependence of exchange probability on physical parameters such as the bond force arises naturally and does not have to be manually added into an acceptance criterion.

Fig. 4 shows the swap rate decreases by two orders of magnitude when $\beta\Delta E_{\text{sw}}$ is increased from zero to six, correlated with the rise of the elastic plateau in the stress relaxation modulus $G(t)$. Thus, $\beta\Delta E_{\text{sw}}$ controls the solid-liquid transition or topological glass transition in the same way catalyst concentration or temperature do this in experiments.

Applying this method to two different mixtures, we demonstrate the importance of topological considerations for stress relaxation, extending recent insights into the effect of loop-like defects on static elastic properties [16, 31]. With the same number of swapping events, our primary-loop-free mixture of star polymers relaxes stress much more slowly than the loopy mixture of otherwise similar star polymers.

We stress the peculiar role for doubly connected stars in these networks: For the static modulus, there is little difference between a single or double polymer bridge between two star centers, as each bridge in a second-order loop is about half as effective as a single bridge [16]. When it comes to relaxing stresses via swapping, how-

ever, the doubly connected stars contribute much more slowly since the force between them will only be relaxed away after both bonds have undergone a swap.

Interestingly, we found that we can exert some control over how many loops are formed in the defect-allowing mixture by way of excluded volume interactions, temperature and deformation as we show in Fig. 5. This observation may open up ways to enhance control over the elastic properties of networks, which is a topic that deserves further study in the context of vitrimers and other bond-swapping materials.

While in standard cross-linked networks the density of loops can be controlled through the reaction protocol [31], we speculate that the state at which a vitrimer is allowed to equilibrate topologically, determines the number of defects at equilibrium. If we then do a rapid temperature quench to a regime where bond exchange is inhibited, the topology is frozen in a state with a controlled average number of defects.

In summary, our results suggest that novel vitrimer systems can be designed explicitly considering defects as a means to control mechanical properties. This class of polymeric materials will then, on top of their recyclability and their remarkable ability to recover their initial properties after remolding, also become mechanically tunable.

Acknowledgments—We are grateful to Hans Heuts and Cornelis Storm for helpful comments.

-
- [1] M. Rubinstein and R. H. Colby, *Polymer physics*, Vol. 23 (Oxford University Press New York, 2003).
- [2] C. J. Kloxin and C. N. Bowman, *Chem Soc Rev* **42**, 7161 (2013).
- [3] W. Denissen, J. M. Winne, and F. E. Du Prez, *Chem Sci* **7**, 30 (2016).
- [4] D. Montarnal, M. Capelot, F. Tournilhac, and L. Leibler, *Science* **334**, 965 (2011).
- [5] M. Capelot, D. Montarnal, F. Tournilhac, and L. Leibler, *J Am Chem Soc* **134**, 7664 (2012).
- [6] E. Chabert, J. Vial, J.-P. Cauchois, M. Mihaluta, and F. Tournilhac, *Soft Matter* **12**, 4838 (2016).
- [7] Q. Chen, X. Yu, Z. Pei, Y. Yang, Y. Wei, and Y. Ji, *Chem. Sci.* **8**, 724 (2017).
- [8] Z. Yang, Q. Wang, and T. Wang, *ACS Appl. Mater. Inter.* **8**, 21691 (2016).
- [9] A. Ruiz de Luzuriaga, J. M. Matxain, F. Ruipérez, R. Martín, J. M. Asua, G. Cabañero, and I. Odriozola, *J. Mater. Chem. C* **4**, 6220 (2016).
- [10] A. C. Van Duin, S. Dasgupta, F. Lorant, and W. A. Goddard, *J Phys Chem A* **105**, 9396 (2001).
- [11] J. P. Wittmer, I. Kriuchevskiy, A. Cavallo, H. Xu, and J. Baschnagel, *Phys Rev E* **93**, 062611 (2016).
- [12] E. B. Stukalin, L.-H. Cai, N. A. Kumar, L. Leibler, and M. Rubinstein, *Macromolecules* **46**, 7525 (2013).
- [13] F. Smalenburg, L. Leibler, and F. Sciortino, *Phys Rev Lett* **111**, 188002 (2013).
- [14] F. Sciortino, *Eur. Phys. J. E* **40**, 3 (2017).
- [15] F. Snijkers, R. Pasquino, and A. Maffezzoli, *Soft Matter* **13**, 258 (2017).
- [16] M. Zhong, R. Wang, K. Kawamoto, B. D. Olsen, and J. A. Johnson, *Science* **353**, 1264 (2016).
- [17] L. Rovigatti, G. Nava, T. Bellini, and F. Sciortino, *Macromolecules* (2018).
- [18] Z. S. Kean, J. L. Hawk, S. Lin, X. Zhao, R. P. Sijbesma, and S. L. Craig, *Adv Mater* **26**, 6013 (2014).
- [19] E. Ducrot, Y. Chen, M. Bulters, R. P. Sijbesma, and C. Creton, *Science* **344**, 186 (2014).
- [20] T. Sakai, T. Matsunaga, Y. Yamamoto, C. Ito, R. Yoshida, S. Suzuki, N. Sasaki, M. Shibayama, and U. I. Chung, *Macromolecules* **41**, 5379 (2008).
- [21] T. Matsunaga, T. Sakai, Y. Akagi, U.-i. Chung, and M. Shibayama, *Macromolecules* **42**, 1344 (2009).
- [22] K. Kremer and G. S. Grest, *J Chem Phys* **92**, 5057 (1990).
- [23] J. D. Weeks, D. Chandler, and H. C. Andersen, *J. Chem. Phys.* **54**, 5237 (1971).
- [24] J. A. Anderson, C. D. Lorenz, and A. Travesset, *J Comput Phys* **227**, 5342 (2008).
- [25] J. Glaser, T. D. Nguyen, J. A. Anderson, P. Lui, F. Spiga, J. A. Millan, D. C. Morse, and S. C. Glotzer, *Comput Phys Commun* **192**, 97 (2015).
- [26] See Supplementary info (number to be added by editor).
- [27] J. P. Wittmer, H. Xu, and J. Baschnagel, *Phys Rev E* **91**, 022107 (2015).
- [28] I. Kriuchevskiy, J. P. Wittmer, O. Benzerara, H. Meyer, and J. Baschnagel, *Eur. Phys. J. E* **40**, 43 (2017).
- [29] P. E. Rouse Jr, *J Chem Phys* **21**, 1272 (1953).
- [30] F. Bomboi, F. Romano, M. Leo, J. Fernandez-Castanon, R. Cerbino, T. Bellini, F. Bordini, P. Filetici, and F. Sciortino, *Nat Commun* **7**, 13191 (2016).
- [31] R. Wang, J. A. Johnson, and B. D. Olsen, *Macromolecules* **50**, 2556 (2017).
- [32] W. Denissen, G. Rivero, R. Nicolaÿ, L. Leibler, J. M. Winne, and F. E. Du Prez, *Advanced Functional Materials* **25**, 2451 (2015).
- [33] We use the value $\tau_{\text{liq}} \approx 1 \mu\text{s}$ which is the fastest relaxation time that we get along the protocol. Using instead $\tau_{\text{liq}}(\phi)$ would provide the same correlation for all of the liquid states.
- [34] Y.-X. Lu and Z. Guan, *Journal of the American Chemical Society* **134**, 14226 (2012).
- [35] J.-P. Hansen and I. R. McDonald, *Theory of simple liquids* (Elsevier, 1990).
- [36] J.-L. Barrat and J.-P. Hansen, *Basic concepts for simple and complex liquids* (Cambridge University Press, 2003).
- [37] L. D. Landau and E. Lifshitz, *Course of Theoretical Physics* **3**, 109 (1986).
- [38] Keep in mind the assumption of isotropy that produces a factor 3 in eq.27, making the two expressions identical.

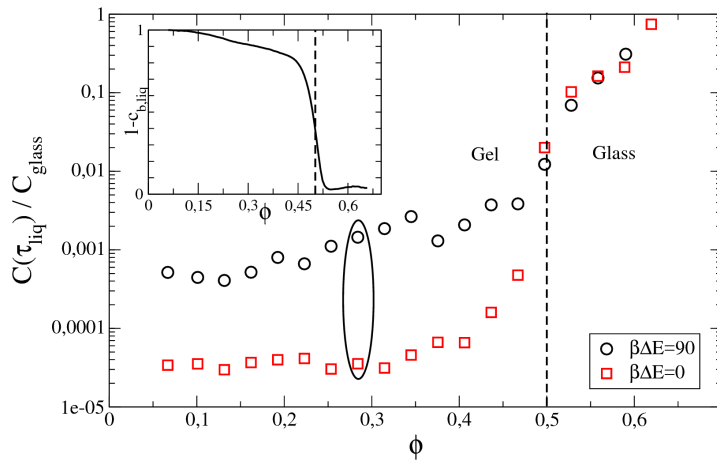


FIG. 6. Long time limit of the stress relaxation function (DAM) as a function of density. In the inset we plot the bond de-correlation function at $\tau_{\text{liq}} \approx 1 \mu\text{s}$. Above the glass transition bond swaps are blocked.

SUPPLEMENTAL INFORMATION included as appendices

APPENDIX A — Two glass transitions

Vitrimers are usually described as systems with two glass transitions. The standard glass transition describes how chains or parts thereof become kinetically arrested upon lowering temperature or increasing density, and happens in melts and crosslinked networks alike. The second glass transition is specific to vitrimers and describes topological arrest. When conditions allow bond swapping, vitrimers are able to rearrange their network structure following a valley-rich path in a rough energy landscape. Without swapping, the network is stuck in a particular topology (polymer architecture). In experiments this topological glass transition is controlled through temperature and catalyst concentration [5, 32]. In our model, correspondingly, through the activation energy for swap $\beta\Delta E_{\text{sw}}$.

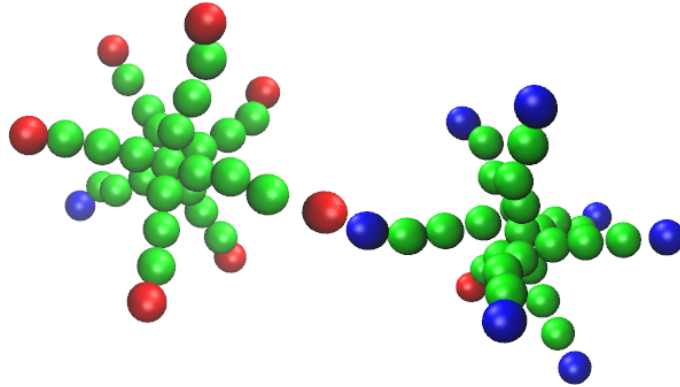
Hence at high temperatures, vitrimers can flow like viscoelastic liquids [3, 15], while they become solid at low temperature or high density through a standard glass transition or at low swap rate through a topological one. The interesting physics of vitrimers is related to their unique topological glass transition, which being reversible and easily controllable in experiments, opens up to a lot of technological and industrial applications [6–9].

To demonstrate that we are looking only at the effects of the topological glass transition we estimated the density at which the standard kinetic glass transition happens. We plot in Fig. 6 the long time limit of $C(t)$ during a compression/decompression protocol. The protocol consists in the equilibration of the same 100 DAM networks with $\beta\Delta E_{\text{sw}} = 0$ at different volumes for a time $t \approx 10\tau_{\text{liq}}$, and then a measure of the stress relaxation $C(\tau_{\text{liq}})$ [33] for both viscous liquids ($\beta\Delta E_{\text{sw}} = 0$) and topologically frozen gels ($\beta\Delta E_{\text{sw}} = 90$). We express our results as a function of effective hard sphere packing fraction, defining $V_{\text{WCA}}(\sigma_{\text{HS}}) = k_{\text{B}}T$. We go from $\phi \approx 0.3$ to $\phi_{\text{max}} \approx 0.61$, which is the point where the equilibration time becomes $t_{\text{eq}} \gg 10\tau_{\text{liq}}$. While decompressing we go down to $\phi \approx 0.05$. The dotted line in Fig. 6 corresponds to $\phi = 0.5$. We can see from the plot that the system behaves the same up until crossing $\phi = 0.5$ where the slowdown starts and the caging effect prevents a full relaxation. After this point in fact, even the $\beta\Delta E_{\text{sw}} = 0$ networks behave as solids. We then measure the bond autocorrelation function $c_b(t)$, which we use to plot the long time limit of the de-correlation function $1 - c_b(\tau_{\text{liq}})$ in the inset of Fig. 6. As hypothesized, above the glass transition bond swaps have no effect. The choice of $\phi \approx 0.3$ that we do in the main text, corresponds to the points in the black ellipse, where the density is low enough to exclude any interference of the glass transition, so that bond-swap-induced structural rearrangements can contribute to stress relaxation.

APPENDIX B — Pressure and stress in the presence of three body interactions

The potential that we want to model between two active sites (i.e. a blue and a red bead in Fig.7) has to be steep and strong in order to capture the strength of ester [5], amide [32], alkene [34] or any bond that can produce vitrimers.

FIG. 7. The typical bond of a vitrimer has to resist thermal fluctuations, but it has to allow swap if a triplet is established.



We base our model on a generalized Lennard-Jones (gLJ)

$$v_{ij}^{(2b)}(\vec{r}_{ij}) = v_{ij}^{(gLJ)}(\vec{r}_{ij}) = \begin{cases} 4\epsilon \left[\left(\frac{\sigma}{r_{ij}} \right)^{20} - \left(\frac{\sigma}{r_{ij}} \right)^{10} \right] & r_{ij} < r_{\text{cut}} \\ 0 & r_{ij} \geq r_{\text{cut}} \end{cases} \quad (6)$$

where we set $\epsilon = 1$, $\sigma = 1$ and at $r_{\text{cut}} = 2.5\sigma$. This is the attraction we impose between active sites to assemble the network. With just this attraction the system would inevitably clusterize, driven by multiple bond formation. We both prevent clusterization and provide a way to model the swapping processes simply combining that gLJ with a three body potential based on the same gLJ:

$$V^{(3b)} = \lambda\epsilon \sum_{ijk} \hat{v}_{ij}^{(2b)}(\vec{r}_{ij}) \cdot \hat{v}_{ik}^{(2b)}(\vec{r}_{ij}) \quad (7)$$

where $\hat{v}_{ij}^{(2b)}$ is an auxiliary potential defined as:

$$\hat{v}_{ij}^{(2b)}(\vec{r}_{ij}) = \begin{cases} 1 & r_{ij} \leq r_{\text{min}} \\ -\frac{v_{ij}^{(2b)}(\vec{r}_{ij})}{\epsilon} & r_{ij} > r_{\text{min}} \end{cases} \quad (8)$$

This solution is not only an elegant and smooth way to model a swap event, but it is also relatively cheap [14]. In fact we only have to combine the standard two body potentials to get the additional three body one, thus no extra computation is required.

It is also more natural to reproduce bond swap in this way compared to a Monte Carlo move, because the three body potential is structured such that a bond which is pulled is more likely to swap. To achieve the same result in MC we should force it using external tuning.

The three body term itself is noticeable only while a bond is swapping (i.e. when three ending beads are within the gLJ cutoff) otherwise it is zero and hence the system is characterized by two body terms only. So the only states that feel the presence of this additional potential are transient triplet states. Our assumption is that during a swap event no more than three sites are involved.

It is of fundamental importance to take those triplet states into account while evaluating thermodynamic quantities, because they deeply characterize the system (in fact without $V^{(3b)}$ we should expect clusterization). Then, in order to estimate the stress relaxation, we have to add those triplet terms in the pressure tensor. To do so we can not rely on the standard virial approach [35] on which MD software are based, because one of its assumption is the pairwise interaction.

In the following, we will derive a general expression for the isotropic pressure at equilibrium that includes the triplet contributions. Lastly we will generalize that expression to its tensorial shape introducing the stress tensor as $\sigma_{\alpha\beta} = -P_{\alpha\beta}$. In this way we are able to measure the stress relaxation as discussed in the main text.

Isotropic pressure

It is possible to evaluate the average pressure in the canonical ensemble at fixed number of molecules N , volume V and temperature T using its definition

$$P \equiv - \left(\frac{\partial F}{\partial V} \right)_{T,N} \quad (9)$$

and expressing the free energy F from the partition function Q

$$F = -k_b T \log(Q) \quad (10)$$

then (9) becomes

$$\beta P = \left(\frac{\partial Q}{\partial V} \right)_{T,N} \quad (11)$$

The partition function itself is defined as

$$Q(N, V, T) \equiv \frac{1}{N! h^{3N}} \int d\{r_i\} d\{p_i\} \exp(-\beta H) \quad (12)$$

where H is the Hamiltonian that describes our system. It is possible to integrate analytically the momenta because their only dependence in the Hamiltonian is through the kinetic energy and that produces a gaussian integral. So we get

$$Q(N, V, T) = \frac{1}{N! \lambda_T^{3N}} \int d\{r_i\} \exp(-\beta U(\{r_i\})) \quad (13)$$

where the thermal wavelength corresponds to $\lambda_T = h/\sqrt{2\pi m k_B T}$.

To get the pressure we have to take a derivative with respect to V but the volume dependence is not only in the potential U , but also in the integration boundaries for the positions $\{r_i\}$. A solution is to use this new set of scaled variables

$$\xi_i \equiv \frac{r_i}{L} \quad (14)$$

defined in this way to isolate the V dependence from the integration domain. In fact (13) becomes now

$$Q(N, V, T) = \frac{V^N}{N! \lambda_T^{3N}} \int_0^1 d\{\xi_i\} \exp(-\beta U(\{\xi_i\}, V)) \quad (15)$$

and we can finally derive the right side of (11)

$$\beta P = \frac{1}{Q} \frac{\partial Q}{\partial V} \quad (16)$$

$$= \frac{N}{V} - \beta \left\langle \frac{\partial U}{\partial V} \right\rangle \quad (17)$$

where the bracket $\langle \cdot \rangle$ denotes the ensemble average. If at this point we separate the two and three body potentials we get that

$$\beta P = \frac{N}{V} - \beta \left\langle \frac{\partial v^{(2b)}}{\partial V} \right\rangle - \beta \left\langle \frac{\partial v^{(3b)}}{\partial V} \right\rangle \quad (18)$$

$$= \beta P^{(2b)} + \beta P^{(3b)} \quad (19)$$

$P^{(2b)}$ is the standard pressure tensor in virial-2body approximation, which is widely discussed in any soft matter textbook [35, 36]. Instead $P^{(3b)}$, which is usually assumed to be zero, now requires a more detailed evaluation.

Factorizable 3 body potential - The three body potential in (7) is not a general function of three variables. Its three body dependence is only through the sum of products of two variables at the time. Hence, there are no terms like $x_i x_j x_k$. This means that its derivatives can be simplified further dividing each terms of the sum into two:

$$\frac{\partial v^{(3b)}}{\partial V} = \frac{1}{3L^2} \frac{\partial v^{(3b)}}{\partial L} \quad (20)$$

$$= \frac{1}{3L^2} \frac{\partial}{\partial L} \left[\sum_{ijk}^* \lambda \epsilon \hat{v}_{ij}^{(2b)} \cdot \hat{v}_{ik}^{(2b)} \right] \quad (21)$$

$$= \frac{\lambda \epsilon}{3L^2} \sum_{ijk}^* \left[\frac{\partial \hat{v}_{ij}^{(2b)}}{\partial L} \cdot \hat{v}_{ik}^{(2b)} + \hat{v}_{ij}^{(2b)} \cdot \frac{\partial \hat{v}_{ik}^{(2b)}}{\partial L} \right] \quad (22)$$

With \sum_{ijk}^* we mean that the summation has to be limited to the distinct triplets to avoid over counting. The derivatives of \hat{v} are

$$\frac{\partial \hat{v}^{(2b)}(r_{ab})}{\partial L} = \frac{\partial \hat{v}^{(2b)}(r_{ab})}{\partial x_{ab}} \frac{\partial x_{ab}}{\partial L} + \frac{\partial \hat{v}^{(2b)}(r_{ab})}{\partial y_{ab}} \frac{\partial y_{ab}}{\partial L} + \frac{\partial \hat{v}^{(2b)}(r_{ab})}{\partial z_{ab}} \frac{\partial z_{ab}}{\partial L} \quad (23)$$

Due to the fact that $\vec{r}_{ab} \equiv L \vec{\xi}_{ab}$ we have for each of the component of (18)

$$\frac{\partial r_\alpha}{\partial L} = \xi_\alpha = \frac{r_\alpha}{L} \quad (24)$$

and then

$$\frac{\partial \hat{v}^{(2b)}(r_{ab})}{\partial L} = -\vec{F}_{ab} \cdot \frac{\vec{r}_{ab}}{L} \quad (25)$$

Substituting (20) in (17) follows that

$$\frac{\partial v^{(3b)}}{\partial V} = -\frac{\lambda \epsilon}{3L^3} \sum_{ijk}^* \left[\vec{F}_{ij} \cdot \vec{r}_{ij} \hat{v}_{ik}^{(2b)} + \hat{v}_{ij}^{(2b)} \vec{F}_{ik} \cdot \vec{r}_{ik} \right] \quad (26)$$

and then the total pressure

$$\beta P = \beta P_{\text{virial}}^{(2b)} + \beta \frac{\lambda \epsilon}{3L^3} \sum_{ijk}^* \left[\vec{F}_{ij} \cdot \vec{r}_{ij} \hat{v}_{ik}^{(2b)} + \hat{v}_{ij}^{(2b)} \vec{F}_{ik} \cdot \vec{r}_{ik} \right] \quad (27)$$

The main advantages of our 3 body potential is still shining in this formula in fact we already know all \vec{F}_{ij} because we had to evaluate them for the dynamics of the system. So this expression is computationally cheap.

Pressure and Stress tensor

A formal expression for the stress tensor in the presence of our 3-body factorizable interaction can be derived in the framework of elasticity theory [37]. A general deformation of a solid body can be defined as a transformation for its points $\mathbf{r}'_\alpha \equiv \Lambda_{\alpha\beta} \mathbf{r}_\beta$, where $\Lambda_{\alpha\beta}$ is the deformation tensor and α and β represent the components x, y, z in Einstein notation. It follows that any point is displaced by $\mathbf{u} \equiv \mathbf{r}' - \mathbf{r}$ where we introduced the displacement field \mathbf{u} . When an object is deformed the vector joining the same two points, called dl , is deformed as well. Following Landau, in hypothesis of small deformation, we get that

$$(dl')^2 = dl^2 + 2u_{ik} dx_i dx_k \quad (28)$$

u_{ik} is an important quantity called the linearized strain tensor and defined by:

$$u_{ik} \equiv \frac{1}{2} \left(\frac{\partial u_i}{\partial x_k} + \frac{\partial u_k}{\partial x_i} \right) \quad (29)$$

From its definition it is clear that it is symmetrical. It then means that it can be diagonalized at any point, i.e. we can choose co-ordinates axes in such a way that only u_{ii} components of the tensors are non-zero (this will come in handy later on).

When a deformation occurs the arrangement of the molecules changes, hence thermal and mechanical equilibrium are broken. As a response, some portions of the body are going to have a resultant force different from zero that would like to rearrange the body in a new equilibrium. These internal forces produce the so called internal stress σ_{ij} . It is possible to evaluate those forces [37] and determine them from the work done by the deformation $\delta W = -\sigma_{ik}\delta u_{ik}$. Its contribute to the internal energy is $dE = TdS + \sigma_{ik}du_{ik}$. Assuming instantaneous equilibrium we can introduce a free energy $F = E - TS$ that for the deformed solid becomes

$$dF = -SdT + \sigma_{ik}du_{ik} \quad (30)$$

This allows us to get an expression for the stress tensor

$$\sigma_{ik} = \left(\frac{\partial F}{\partial u_{ik}} \right)_T \quad (31)$$

Diagonal terms - For the diagonal terms $k = i$, the strain tensor and the stress are

$$u_{ii} = \frac{\partial u_i}{\partial x_i} = \Lambda_{ii} \quad (32)$$

$$\Rightarrow \sigma_{ii} = \frac{\partial F}{\partial u_{ii}} \quad (33)$$

$$= \frac{\partial F}{\partial \Lambda_{ii}} \quad (34)$$

$$= \frac{\partial F}{\partial x'_i} \frac{\partial x'_i}{\partial \Lambda_{ii}} + \frac{\partial F}{\partial V'} \frac{\partial V'}{\partial \Lambda_{ii}} \quad (35)$$

$$= \frac{\partial F}{\partial x'_i} x_i + \frac{\partial F}{\partial V'} V \quad (36)$$

$$\approx \frac{\partial F}{\partial x'_i} x'_i + \frac{\partial F}{\partial V} V \quad (37)$$

to handle the derivative of the volume V we used the fact that $V' = V + \Lambda_{ii}V + o(\Lambda^2)$, then assumed small deformation, hence $\Lambda \ll 1$ and $x \approx x'$. So we get for the the $i = x$ component

$$\sigma_{xx} = \frac{1}{V} \left(\frac{\partial F}{\partial x} x + \frac{\partial F}{\partial V} V \right) \quad (38)$$

where we normalized the stress dividing it by the entire volume V of the system. The stress tensor can be rewritten in this form

$$\sigma_{ij} = -P\delta_{ij} + \sigma_{ij}^d \quad (39)$$

$$\equiv -p_{ij} \quad (40)$$

where p_{ij} is the pressure tensor, $P = \frac{1}{3}\text{tr}(p_{ij})$ is the isotropic pressure and σ_{ij}^d is the out of equilibrium dynamical stress. At equilibrium in isotropic condition, the relation states that $\sigma_{ii} = P = p_{jj}$ for any choice of i and j , as it can be easily verified comparing eq.38 with eq.27 [38].

Off-diagonal components - It is also possible to get the off diagonal components of the stress tensor. To do so, we start assuming symmetrical strain $\Lambda_{ij} = \Lambda_{ji} \equiv \Lambda$, then the off diagonal strains are:

$$u_{ij} = \frac{1}{2} \left(\frac{\partial u_i}{\partial x_j} + \frac{\partial u_j}{\partial x_i} \right) = \Lambda \quad (41)$$

and then the stress

$$\sigma_{ij} = \frac{\partial F}{\partial u_{ij}} \quad (42)$$

$$= \frac{\partial F}{\partial r'} \frac{\partial r'}{\partial \Lambda} + \frac{\partial F}{\partial V'} \frac{\partial V'}{\partial \Lambda} \quad (43)$$

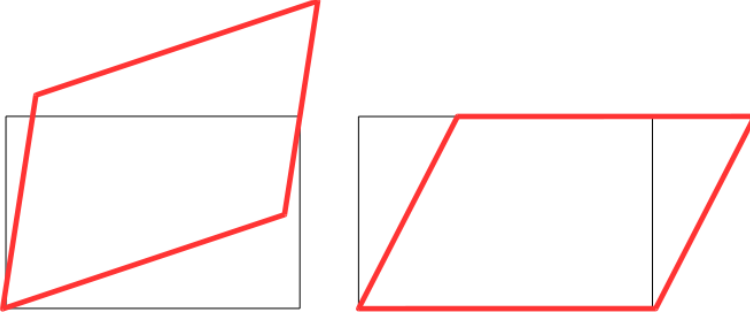


FIG. 8. A solid (black) after a deformation (red) defined by $x' = x + \Lambda z$ and $z' = z + \Lambda x$. The same transformation can be rotated such that it becomes a single component deformation, changing the perspective from left to right. With this approach $x' = x + 2\Lambda z$ but then in eq. (43) we have to take the derivative only for a single direction.

at this point we could evaluate the derivative of the free energy with respect to the strain parameter Λ , but it is easier to follow the argument sketched in Fig. 8. We can see that every off diagonal strain (i.e. one where we mix two components), can be expressed in a simpler way using the rotation depicted in the figure. In this way the Λ dependence is on a single coordinate, hence it is easier to evaluate the derivative. After the rotation eq. (43) becomes

$$\sigma_{ij} = \frac{\partial F}{\partial x_i} \frac{\partial x_i}{\partial \Lambda} + \frac{\partial F}{\partial V'} \frac{\partial V'}{\partial \Lambda} \quad (44)$$

$$= \frac{\partial F}{\partial x_i} x_j + \frac{\partial F}{\partial V'} \frac{\partial V'}{\partial \Lambda} \quad (45)$$

Using the same tricks that we used for the pressure, we can decompose the stress tensor in an ideal gas term, a two body virial like term and a three body term that we evaluate again using factorization. The final expression is then:

$$\sigma_{\alpha\beta} = -P_{\alpha\beta, \text{virial}}^{(2b)} - \frac{\lambda\epsilon}{V} \sum_{ijk}^* \left[\left(\vec{F}_{ij}(r_{ij}) \right)_\alpha (\vec{r}_{ij})_\beta \hat{v}_{ik}^{(2b)} + \hat{v}_{ij}^{(2b)} \left(\vec{F}_{ik}(r_{ik}) \right)_\alpha (\vec{r}_{ik})_\beta \right] \quad (46)$$